

Palladium-Catalyzed Cross-Coupling Reactions of Dithienosilole with Indium Reagents: Synthesis and Characterization of Dithienosilole Derivatives and Their Application to Organic Light-Emitting Diodes

Hwasoon Jung,[§] Hyonseok Hwang,[§] Ki-Min Park,[‡] Jinho Kim,[§] Dong-Ha Kim,^{*,†} and Youngjin Kang^{*,§}

[†]Electronic Material Development Team, Corporate R&D Center, DSHM Co. Ltd., 404-1 Baekhyun-Dong, Bundang-Gu, Sungnam-City, Kyunggi-Do 463-420, Republic of Korea, [‡]Department of Chemistry & Research Institute of Natural Science, Gyeongsang National University, Jinju 660-701, Republic of Korea, and [§]Department of Chemistry and Division of Science Education, Kangwon National University, Chuncheon 200-701, Republic of Korea

Received March 23, 2010

Three dithienosilole (DTS) derivatives bearing naphthyl segments, 5,5'-dinaphthyl-1,1-dimethyldithienosilole (**1**), 5,5'-dinaphthyl-1-methyl-1-phenyldithienosilole (**2**), and 5,5'-dinaphthyl-1,1-diphenyldithienosilole (**3**), are prepared through Pd(II)-catalyzed cross-coupling using an organoindium reagent as a nucleophile. The molecular structure of **3** is confirmed by single-crystal X-ray analysis. In addition, thermal, photophysical, and electrochemical properties for all three compounds are systematically investigated. The introduction of naphthyl segments into the DTS framework leads to an excellent enhancement of thermal stability with relatively high glass transition (T_g : 87 °C) and decomposition temperatures (T_d : 320–380 °C). A red shift in both absorption and emission is observed in the DTS series as the 1,1-substituents on the ring silicon atom become more electronegative. On the basis of absorption spectra and DFT/TDDFT calculations, intense green photoluminescence observed for all compounds can be attributed to the effective π - π^* transition of the DTS and naphthyl group with a small contribution of the σ^* orbital of the exocyclic Si-C bond. The electron-transporting properties of **1**, **2**, and **3** were evaluated by the performance of organic light-emitting diodes (OLEDs), comprising 4,4',4''-tris(*N*-(2-naphthyl)-*N*-phenylamino)triphenylamine (2-TNA-TA) as hole-injection layer, 4,4'-bis(*N*-phenyl-1-naphthylamino)biphenyl (NPB) as hole-transport layer, 10-(2-benzothiazolyl)-1,1,7,7-tetramethyl-2,3,6,7-tetrahydro-1*H*,5*H*,11*H*-benzo[*l*]pyrano[6,7-*ij*]quinolizin-11-one (C545T)/tris(8-quinolinato)aluminum (Alq₃) as emitting layer, and the DTS series as electron-transporting layer, respectively. The device shows intense green emission with a high efficiency of 8.0 cd/A at 1000 cd/m².

Introduction

Organosilicon compounds based on silole (silacyclopentadiene) have become an interesting subject in materials science due to their varied applications, such as in conductors, sensors, and OLEDs (organic light-emitting diodes).¹ Especially, silole derivatives have been shown to be an excellent electron-transporting material for OLEDs because they possess a low-lying LUMO due to the interaction between the σ^* orbital of their two exocyclic Si-C bonds and the π^* orbitals of the butadiene moiety.² Silole derivatives that exhibit emission from blue to orange-red by the incorporation of various substituents at the 2 and 5 positions of the silole ring have been reported previously.

It has been found that the photophysical properties and electronic structures of a silole significantly depend on the nature of the 2,5-substituents.³ Moreover, silole derivatives have been shown to have a very good efficiency in electroluminescence (EL) devices.⁴ So far, siloles being used for OLEDs could be divided into five classes: 1-functionalized tetraphenylsilole (type 1),^{4a,5} 2,5-functionalized siloles (type 2),^{4b,6} 5,5'-functionalized

*To whom correspondence should be addressed. E-mail: kangy@kangwon.ac.kr.

(1) (a) Recent review: Zhan, X.; Barlow, S.; Marder, S. R. *Chem. Commun.* **2009**, 1948, and references therein. (b) Sohn, H.; Sailor, M. J.; Magde, D.; Trogler, W. C. *J. Am. Chem. Soc.* **2003**, *125*, 3821. (c) Usta, H.; Lu, G.; Facchetti, A.; Marks, T. J. *J. Am. Chem. Soc.* **2006**, *128*, 9034. (d) Wang, Y.; Hou, L.; Yang, K.; Chen, J.; Wang, F.; Cao, Y. *Macromol. Chem. Phys.* **2005**, *206*, 2190.

(2) Yamaguchi, S.; Tamao, K. *Bull. Chem. Soc. Jpn.* **1996**, *69*, 2327.

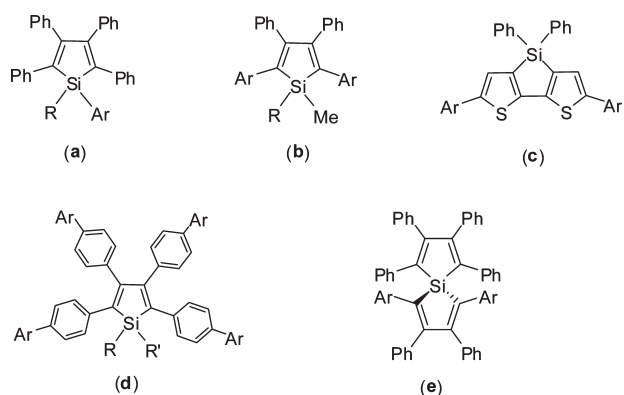
(3) (a) Lee, J.; Liu, Q.; Motala, M.; Dane, J.; Gao, J.; Kang, Y.; Wang, S. *Chem. Mater.* **2004**, *16*, 1869. (b) Boydston, A. J.; Yin, Y.; Pagenkopf, B. L. *J. Am. Chem. Soc.* **2004**, *126*, 3724.

(4) (a) Chen, H. Y.; Lam, W. Y.; Luo, J. D.; Ho, Y. L.; Tang, B. Z.; Zhu, D. B.; Wong, M.; Kwok, H. S. *Appl. Phys. Lett.* **2002**, *81*, 574. (b) Murata, H.; Kafafi, Z. H.; Uchida, M. *Appl. Phys. Lett.* **2002**, *80*, 189.

(5) (a) Tang, B. Z.; Zhan, X. W.; Yu, G.; Lee, P. P. S.; Liu, Y. Q.; Zhu, D. B. *J. Mater. Chem.* **2001**, *11*, 2974. (b) Chen, J.; Law, C. C. W.; Lam, J. W. Y.; Dong, Y.; Lo, S. M. F.; Williams, I. D.; Zhu, D.; Tang, B. Z. *Chem. Mater.* **2003**, *15*, 1535.

(6) (a) Zhan, X.; Haldi, A.; Risko, C.; Chan, C. K.; Zhao, W.; Timofeeva, T. V.; Korlyukov, A.; Antipin, M. Y.; Montgomery, S.; Thompson, E.; An, Z.; Domercq, B.; Barlow, S.; Kahn, A.; Kippelen, B.; Brédas, J.-L.; Marder, S. R. *J. Mater. Chem.* **2008**, *18*, 3157. (b) Uchida, M.; Izumizawa, T.; Nakano, T.; Yamaguchi, S.; Tamao, K.; Furukawa, K. *Chem. Mater.* **2001**, *13*, 2680. (c) Tamao, K.; Uchida, M.; Izumizawa, T.; Fukukawa, K.; Yamaguchi, S. *J. Am. Chem. Soc.* **1996**, *118*, 11974.

Chart 1. Molecular Structures of Representative Silole Derivatives Being Used for OLEDs: (a) Type 1, (b) Type 2, (c) Type 3, (d) Type 4, (e) Type 5^a



^a Ar: either phenyl or functionalized aromatic group.

dithienosiloles (type 3),⁷ 2,3,4,5-tetrafunctionalized siloles (type 4),⁸ and 2,5-functionalized spiro-bisiloles (type 5),⁹ as shown in Chart 1.

The external quantum efficiency (EQE) of OLEDs fabricated by using siloles as emissive or electron-transporting materials ranges from 0.0045% to 8%.^{4a,5a} Such results indicate that the efficiency of silole-based OLEDs is quite sensitive to both the device structure and the molecular structure of the siloles. Therefore, continuous efforts for the development of suitable silole derivatives for application in OLEDs and the finding of optimized device conditions are still required.

Recently, a two thiophene fused silole, dithienosilole (DTS), has attracted much attention due to its usefulness as a building block that can be incorporated into conjugated molecules and polymers.¹⁰ Although DTS has a number of advantages, such as the ease of introducing substituents at different positions of the DTS ring, high photoluminescence quantum efficiency in both solution and the solid state, and easy tuning of emission energy, etc., there have been only a few reports on DTS-based OLED performance due to synthetic limitations of DTS derivatives.⁸

To prepare DTS-based π -conjugated compounds, typical coupling reactions, such as Kumada¹¹ and Stille couplings,¹² are mainly adopted. These reactions, however, need harsh reaction conditions and gave either poor or moderate yields.

Therefore, there is still a strong need for a preparative method of DTS-based π -conjugated compounds. We have recently developed palladium(II)-catalyzed cross-coupling using indium reagents.¹³ This method complements the existing synthetic methods due to some advantageous properties of indium reagents such as availability, ease of preparation and handling, high reactivity, operational simplicity, and low toxicity.

For OLED application, molecules should have high thermal stabilities, high quantum yields, and good film-forming properties (glassy nature) in order to obtain high efficiency in OLED performance.¹⁴ Highly π -conjugated compound derivatives bearing a naphthyl segment were not only regarded as promising host materials but also showed high thermal stability and efficiency.¹⁵ In these molecules, the naphthyl group could play a key role in enhancing thermal stability and uniform film-forming properties.^{15a} Therefore, we expected that the combination of a highly fluorescent DTS unit and a naphthyl segment would be the best pathway to develop efficient materials. Herein, we describe the results of our investigation on the preparation, structural characterization, electrochemical behavior, optical properties, and the fabrication of multilayer light-emitting devices of a series of DTS-based π -conjugated compounds bearing a naphthyl moiety.

Result and Discussion

Syntheses and Characterization of Dithienosilole-Bearing Naphthyl Groups. The synthetic route and details for three new DTS derivatives are shown in Scheme 1. In our initial study, we have attempted syntheses of **1–3** using typical cross-coupling methods, Kumada,¹¹ Stille,¹² Negishi,¹⁶ and Suzuki coupling,¹⁷ under mild or reflux conditions according to previous reports. All of these coupling reactions, however, gave **1–3** in poor to moderate yields. Even undesired compounds, silanol and oxo-bridged siloxane-bithiophene, were obtained as major components when used Suzuki coupling. This result is presumably attributed to ring cleavage of the Si–C(thiophene) bond in the presence of base. As an alternative method, we examined a new cross-coupling reaction using indium reagent as a nucleophile in the presence of various palladium catalysts. At first, we examined the stoichiometry of tri(2-naphthyl)indium and the catalytic activity of several palladium catalysts, such as Pd(0) and Pd(II), under varied reaction conditions. Of the conditions screened, the best results were obtained with tri(2-naphthyl)indium (1.0 equiv) in the presence of Pd(dppf)Cl₂ (dppf = 1,1'-bis(diphenylphosphino)ferrocene) in THF (70–80 °C), producing **1–3** in moderate to good yield (50–60%) (details are presented in the Experimental Section; see Scheme 1).

All compounds are stable in air and soluble in common organic solvents but only slightly soluble in hexane and pentane. The structures of **1–3** have been confirmed by ¹H NMR, ¹³C NMR, and mass and elemental analyses, including X-ray diffraction analysis of **3**. In order for molecular organic materials to be useful in EL devices, they should be thermally and morphologically stable.^{14a} Therefore, we performed TGA

(7) (a) Ohshita, J.; Kai, H.; Takada, A.; Iida, T.; Kunai, A.; Ohta, N.; Komaguchi, K.; Shiotani, M.; Adachi, A.; Sakamaki, K.; Okita, K. *Organometallics* **2001**, *20*, 4800. (b) Son, H. J.; Han, W. S.; Chun, J. Y.; Kwon, S. N.; Ko, J.; Kang, S. O. *Organometallics* **2008**, *27*, 2464. (c) Ohshita, J.; Kai, H.; Sumida, T.; Kunai, A.; Adachi, A.; Sakamaki, K.; Okita, K. *J. Organomet. Chem.* **2002**, *642*, 137.

(8) Lee, J.; Liu, Q. D.; Bai, D. R.; Kang, Y.; Tao, Y.; Wang, S. *Organometallics* **2004**, *23*, 6205.

(9) (a) Lee, J.; Yuan, Y. Y.; Kang, Y.; Jia, W.-L.; Lu, Z.-H.; Wang, S. *Adv. Funct. Mater.* **2006**, *16*, 681. (b) Lee, H.; Kim, J.; Kang, Y. *Inorg. Chem. Commun.* **2007**, *10*, 731.

(10) (a) Kim, D.-H.; Ohshita, J.; Lee, K.-H.; Kunugi, Y.; Kunai, A. *Organometallics* **2006**, *25*, 1511. (b) Lee, T.; Jung, I.; Song, K. H.; Lee, H.; Choi, J.; Lee, K.; Lee, B. J.; Pak, J. Y.; Lee, C.; Kang, S. O.; Ko, J. *Organometallics* **2004**, *23*, 5280. (c) Ohshita, J.; Nodono, M.; Watanabe, T.; Ueno, Y.; Kunai, A.; Harima, Y.; Yamashita, K.; Ishikawa, M. *J. Organomet. Chem.* **1998**, *553*, 487. (d) Ohshita, J.; Lee, K.-H.; Hamamoto, D.; Kunugi, Y.; Ikada, J.; Kwak, Y.-W.; Kunai, A. *Chem. Lett.* **2004**, *33*, 892. (e) Ohshita, J.; Lee, K.-H.; Kimura, K.; Kunai, A. *Organometallics* **2004**, *23*, 5622.

(11) Tamao, K.; Kodama, S.; Nishimura, I.; Kumada, M.; Minato, A. *Tetrahedron* **1982**, *38*, 3347.

(12) Stille, J. K. *Angew. Chem., Int. Ed. Engl.* **1986**, *25*, 508.

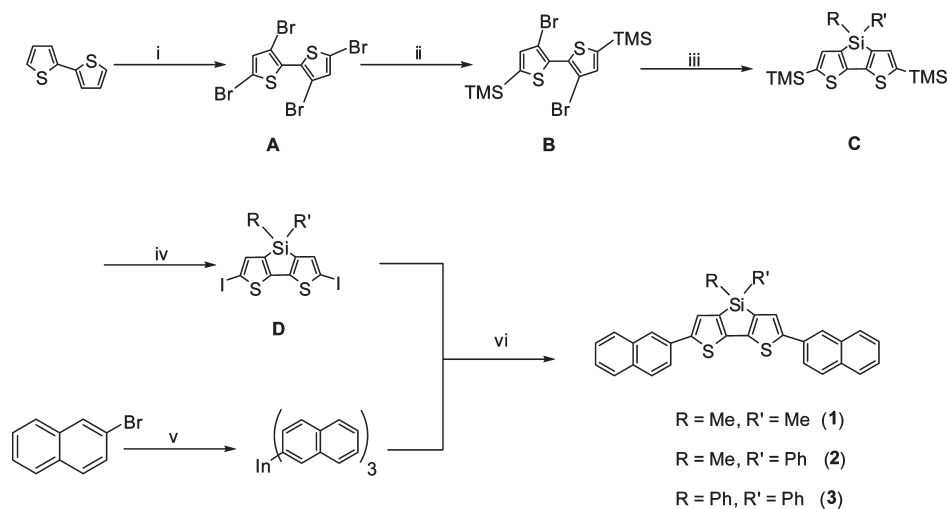
(13) Lee, W.; Kang, Y.; Lee, P. H. *J. Org. Chem.* **2008**, *73*, 4326.

(14) (a) Shirota, Y. *J. Mater. Chem.* **2005**, *15*, 75. (b) Tokito, S.; Iijima, T.; Suzuri, Y.; Kita, H.; Tsuzuki, T.; Sato, F. *Appl. Phys. Lett.* **2003**, *83*, 569.

(15) (a) Bonvallet, P. A.; Breitzkreuz, C. J.; Kim, Y. S.; Todd, E. M.; Traynor, K.; Fry, C. G.; Ediger, M. D.; McMahon, R. J. *J. Org. Chem.* **2007**, *72*, 10051. (b) Lee, J.-H.; Ho, Y.-H.; Lin, T.-C.; Wu, C.-F. *J. Electrochem. Soc.* **2007**, *154*, J226. (c) Tang, H.; Li, Y.; Wang, X.; Wang, W.; Sun, R. *Jpn. J. Appl. Phys.* **2007**, *46*, 1722.

(16) Milne, J. E.; Buchwald, S. L. *J. Am. Chem. Soc.* **2004**, *126*, 13028.

(17) Miyaura, N.; Suzuki, A. *Chem. Rev.* **1995**, *95*, 2457.

Scheme 1^a

^a Reagents and conditions: (i) CHCl_3 , CH_3COOH , 4.1 equiv of NBS, reflux, 50 h; (ii) *n*-BuLi in $\text{Et}_2\text{O}/\text{THF}$, 2.1 equiv of TMSCl, 7 h; (iii) *n*-BuLi in THF, 2.1 equiv of $\text{RR}'\text{SiCl}_2$, 7 h; (iv) 2.2 equiv of ICl, 6 h at -90°C ; (v) 2.1 equiv of 2-bromonaphthalene, *n*-BuLi, 40 min at -78°C , 0.7 equiv of InCl_3 , 10 min at 0°C ; (vi) 1 equiv of DTS, 0.04 equiv of $\text{Pd}(\text{dppf})\text{Cl}_2$, reflux 10 h.

(thermogravimetric analysis) and DSC (differential scanning calorimetry) experiments to investigate the thermal stability, glass-transition temperatures, and phase transitions for compounds **1–3**.

All compounds are very stable up to approximately 250°C without degradation under N_2 atmosphere, as shown in Figure 1. The decomposition temperature, which is defined as 5% weight loss, of **1**, **2**, and **3** is 325, 359, and 383°C , respectively. Well-resolved melting transitions were observed in all cases (Table 2). Compounds **1** and **3** did not show either glass or crystalline transition during either the first or second heating cycle. The melting transitions of **1**, **2**, and **3** are at 225, 212, and 301°C , respectively. This suggests that the combination of 1,1'-diphenyl-substituted DTS and the naphthyl unit leads to a dramatic increase in melting transition. As opposed to **1** and **3**, the first heating cycle of **2** revealed a high glass-transition temperature of 87°C with crystallization transition (T_c : 160°C), followed by melting at 212°C . The T_g value observed for **2** is considerably higher than those of other silole derivatives.^{6b,8b,18}

All compounds showed consistent and fully reproducible DSC diagrams during two cycles of heating and cooling, indicating that these compounds are thermally stable up to their melting points.

In general, the glass-transition temperature of the molecules is related to their molecular structures.¹⁹ The molecules with symmetrical structure, relatively high molecular weight, and a rigid aromatic group mostly show high glass-transition temperature. On the basis of this consideration, we believe that high thermal stability including high glass-transition temperature of **1–3** is due to the rigidity of the naphthyl and DTS moieties. The results observed in TGA and DSC make all compounds potentially useful for applications in OLEDs.

To better understand the solid-state nature, a single-crystal X-ray diffraction analysis was conducted for **3**.

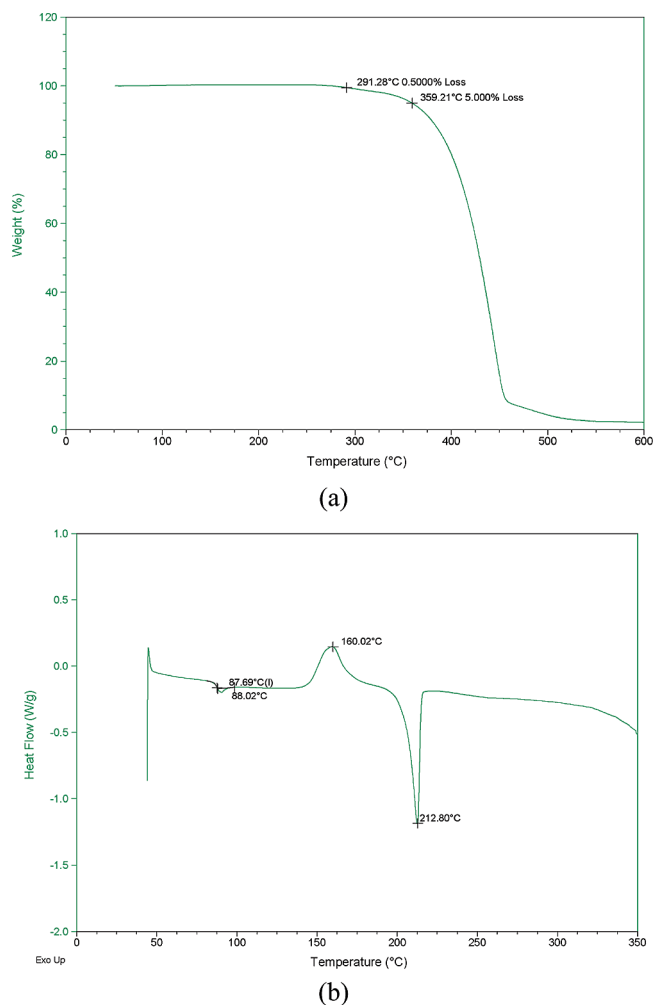


Figure 1. TGA (a) and DSC (b) data of **2**.

Yellow crystals of **3** suitable for X-ray analysis were obtained by the slow evaporation in CH_2Cl_2 and hexane. The crystal data, molecular structure, and selected bond lengths and angles of **3** are presented in Table 1 and Figure 2, respectively.

(18) Yu, G.; Yin, S.; Liu, Y.; Chen, J.; Xu, X.; Sun, X.; Ma, D.; Zhan, X.; Peng, Q.; Shuai, Z.; Tang, B.; Zhu, D.; Fang, W.; Luo, Y. *J. Am. Chem. Soc.* **2005**, *127*, 6335.

(19) (a) Shirota, Y. *J. Mater. Chem.* **2000**, *10*, 1. (b) O'Brien, D. F.; Burrows, P. E.; Forrest, S. R.; Koene, B. E.; Loy, D. E.; Thompson, M. E. *Adv. Mater.* **1998**, *10*, 1108. (c) Koene, B. E.; Loy, D. E.; Thompson, M. E. *Chem. Mater.* **1998**, *10*, 2235.

Table 1. Crystal and Experimental Data for 3

| | |
|--|---|
| formula | C ₄₀ H ₂₆ S ₂ Si |
| fw | 598.82 |
| cryst syst | monoclinic |
| space group | C2/c |
| a (Å) | 28.1771(7) |
| b (Å) | 8.5466(2) |
| c (Å) | 25.1981(6) |
| β (deg) | 92.5110(10) |
| V (Å ³) | 6062.3(3) |
| Z | 8 |
| D _{calc} (g/cm ³) | 1.312 |
| μ (mm ⁻¹) | 0.244 |
| 2θ _{max} (deg) | 56.5 |
| reflns collected | 27 897 |
| indep reflns | 7505 [R(int) = 0.0298] |
| goodness-of-fit on F ² | 1.025 |
| R ₁ , wR ₂ [I > 2σ(I)] | 0.0434, 0.1062 |
| R ₁ , wR ₂ (all data) | 0.0625, 0.1165 |

As shown in Figure 2, two naphthyl groups are connected by a DTS moiety, and bond lengths and angles are within normal ranges and are in agreement with corresponding parameters described for other DTS analogues.^{10b} Interestingly, the dihedral angles between the DTS ring and the two naphthyl group are not the same. One of the naphthyl segment is almost coplanar to the central DTS ring, while the other one is slightly tilted (dihedral angles between outer naphthyl and central DTS ring: 2.81(5)° for the C1–C10 ring and 17.92(6)° for the C19–C28 rings, respectively). This result is due to a strong C(π)···H interaction between naphthyl and the phenyl ring of a neighboring molecule (C27···H38A; 2.71 Å). These observations, coplanarity and small dihedral angles, indicate that π-conjugation of two outer naphthyl groups via the DTS ring occurs effectively. There are a number of face-to-edge interactions in the crystal packing. As a consequence, compound **3** shows a three-dimensional structure via C(π)···H interactions in the crystal packing, as shown in Figure 3, which may be responsible for the thermal stability of the molecules. As the intra- and intermolecular interactions increased, the thermal stability of the molecules increased gradually.²⁰ Therefore, the thermal stability of **3** may originate from these intermolecular interactions.

Photophysical and Electrochemical Properties. The absorption and normalized photoluminescence (PL) spectra of **1–3** in dilute CH₂Cl₂ measured at room temperature are shown in Figure 4. Their resulting photophysical data are summarized in Table 2.

The absorption spectra **1–3** exhibit intense absorption bands centered at ca. 420 nm. The absorption is similar to those of 5,5'-diaryl-DTSs, such as bis[2-(6-trimethylsilyl)pyridyl]dithienosilole (λ_{max} = 418 nm) and bis[2-(5-trimethylsilyl)thienyl]dithienosilole (λ_{max} = 435 nm), but far red-shifted with respect to 5,5'-dialkyl-DTSs.^{7,10} The absorption pattern of all compounds appeared to be nearly the same either in solution or in thin film, which implies that the origin of electronic transition is almost the same and the effect of substituents at the Si atom on the electronic transition is not significant as well. Only maximum absorption spectra for all compounds are slightly different. The absorption maxima steadily shifted to longer wavelength depending on the electron-accepting nature of substituents on the Si atom: Me–Me (**1**; λ_{max} = 421 nm) < Me–Ph (**2**; λ_{max} = 423 nm) < Ph–Ph (**3**; λ_{max} = 426 nm). The bathochromic shift observed for **3** is clearly caused by the phenyl group introduced onto the Si atom, in that, by a general rule of thumb, the more

electronegative phenyl group rather than the alkyl group induces a red-shifted absorption by an inductive effect. This observation is consistent with a previous study on the effect of electronic transition of 1,1-disubstituted silole.²¹

The emission maxima of compounds **1–3** in solution and as thin films at room temperature appear in the region 480–530 nm (see Figure 4 and Supporting Information). Upon excitation at 380 nm, all compounds showed intense green emissions, which are remarkably red-shifted relative to that of 5,5'-bis-(trimethylsilyl)dithienosiloles (λ_{em} = 425 nm),^{7a} due to the lengthening of the conjugated system with the addition of a naphthyl group to the DTS ring. All three DTS compounds do not show significant spectral changes since the electronic interaction between the substituents of the Si atom or the Si atom and the naphthyl groups on the DTS ring is minimal. The emission maxima also showed similar bathochromic shifts to the absorption observed. The emissions of **1–3** doped in a PMMA polymer film exhibit red shifts of 40–45 nm to those in dilute solution. These red shifts observed in the solid state are likely attributable to the difference in dielectric constant of the environment.²² Small Stokes shifts with similar values were observed in all compounds: 2962 cm⁻¹ (0.37 eV) for **1**, 2979 cm⁻¹ (0.37 eV) for **2**, and 3138 cm⁻¹ (0.39 eV) for **3**. The observed small Stokes shifts may imply that all compounds retain the planar geometry in the excited state.²³ Such an observation also is made for *p*-oligophenylene derivatives that retain the same and planar structure in both the ground and excited state.²⁴ The optical band gaps of all compounds were determined from their corresponding absorption tails in solid-state thin films: 485 nm (2.56 eV) for **1**, 492 nm (2.52 eV) for **2**, and 495 nm (2.50 eV) for **3**. The PL quantum yields (Φ_{PL}) in solution were estimated by using 9,10-diphenylanthracene (DPA) as a reference (Φ_{PL} = 0.9). As compared to that of DPA, all compounds show moderate PL quantum efficiency, which increases in the order **1** > **2** > **3**.

To gain deeper insight into the geometrical configuration and the nature of the luminescence displayed by **1–3**, we performed electronic structure calculations for the compounds in the gas phase. More details for the calculations are provided in the Experimental Section. Figure 5 shows the optimized structures of **1–3**, the HOMO and LUMO energy levels for the optimized structures of **1–3**, and the single-crystal structure of **3** (**3-sc**). In Figure 5a, torsional angles between the DTS ring and each of the two naphthyl groups in the optimized structures are 27.9° for **1**, 27.9° and 28.4° for **2**, and 27.6° for **3**. Compared to **3-sc**, the optimized structure of **3** in the gas phase has larger torsional angles. In Figure 5b, the energy gaps between the HOMO and LUMO levels slightly decrease in the order **1** > **2** > **3** > **3-sc**. As mentioned above, the structure of **3-sc** has smaller torsional angles than **3**, leading to the decrease of the energy gap between the HOMO and LUMO levels with an increase in the conjugation.

Figure 6 presents the isodensity plots of the frontier molecular orbitals of **1–3**. The HOMO levels of all the compounds are mainly π orbitals with dominating contributions from the DTS ring and the two naphthyl groups, whereas

(21) Yamaguchi, S.; Jin, R. Z.; Tamao, K. *J. Organomet. Chem.* **1998**, 559, 73.

(22) Salbeck, J.; Yu, N.; Bauer, J.; Weissortel, F.; Estgen, H. *Synth. Met.* **1997**, 91, 209.

(23) Lee, S. H.; Jang, B. B.; Kafafi, Z. H. *J. Am. Chem. Soc.* **2005**, 127, 9071.

(24) Berlman, I. B. *Handbook of Fluorescence Spectra of Aromatic Molecules*, 2nd ed.; Academic Press: New York, 1971.

(20) Lee, S. J.; Park, K. M.; Yang, K.; Kang, Y. *Inorg. Chem.* **2009**, 48, 1030.

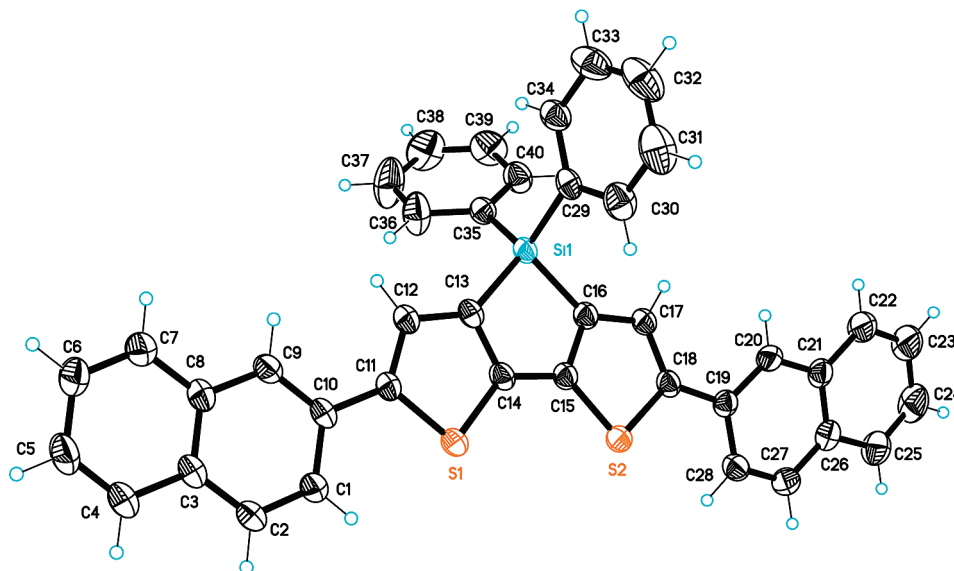


Figure 2. Molecular structure of **3** along with atom-numbering scheme. Selected bond lengths (\AA) and angles (deg): Si(1)–C(35): 1.8593(17), Si(1)–C(16): 1.8687(17), Si(1)–C(29): 1.8692(18), Si(1)–C(13): 1.8723(16), C(35)–Si(1)–C(16): 115.52(8), C(35)–Si(1)–C(29): 109.17(8), C(16)–Si(1)–C(29): 109.27(8), C(35)–Si(1)–C(13): 113.22(8), C(16)–Si(1)–C(13): 91.34(7), C(29)–Si(1)–C(13): 117.51(7).

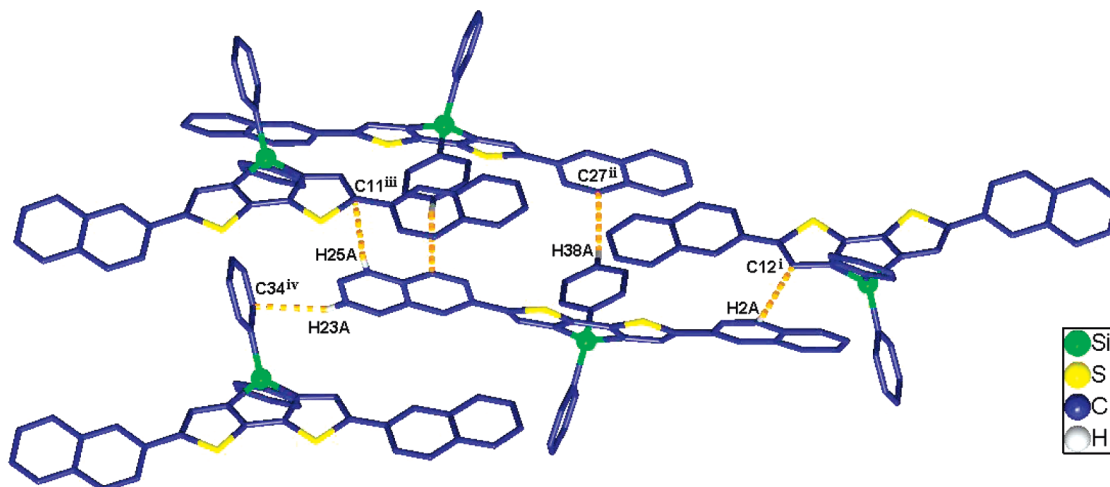


Figure 3. C–H \cdots π interactions in the packing structure of **3** (symmetry codes: (i) $0.5-x, 0.5+y, -0.5-z$; (ii) $-x, 1-y, -z$; (iii) $x, 1-y, 0.5+z$; (iv) $x, -y, 0.5+z$).

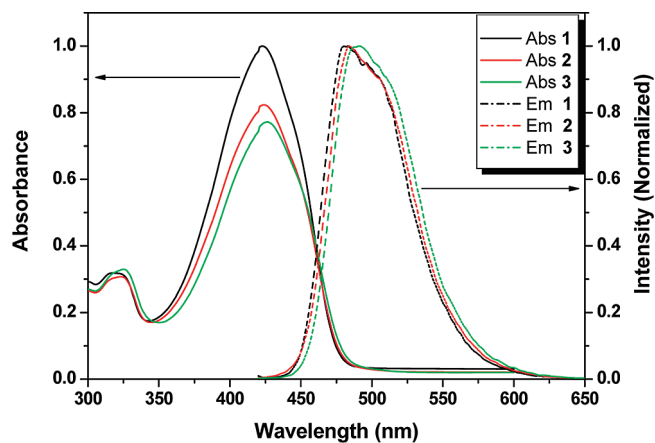


Figure 4. Absorption and emission spectra of **1**, **2**, and **3** in CH_2Cl_2 .

the LUMO levels are largely dominated by π^* orbital contributions from the DTS ring and the two naphthyl groups

with a small contribution from the substituents on the Si atom.

Table 3 shows the calculated $S_0 \rightarrow S_1$ vertical excitation energies along with the oscillator strengths and the transition orbitals having CI coefficients larger than 0.2 for **1–3**. The calculated excitation energies are also compared with the experimental absorption maxima in Table 3. The obtained transition orbitals and significant magnitude of the oscillator strengths as well as the isodensity plots of the HOMO and LUMO levels indicate that the measured absorption and emission spectra of **1–3** can be ascribed to a $\pi-\pi^*$ transition between the DTS and the two naphthyl groups with a small contribution from the substituents on the Si atom. In Table 3, the calculated excitation wavelengths slightly increase from **1** to **3**, agreeing well with the tendency in the experimental absorption maxima. It is also found that the calculated excitation energies are more blue-shifted than the measured absorption bands of the compounds. This may be caused by the fact that the

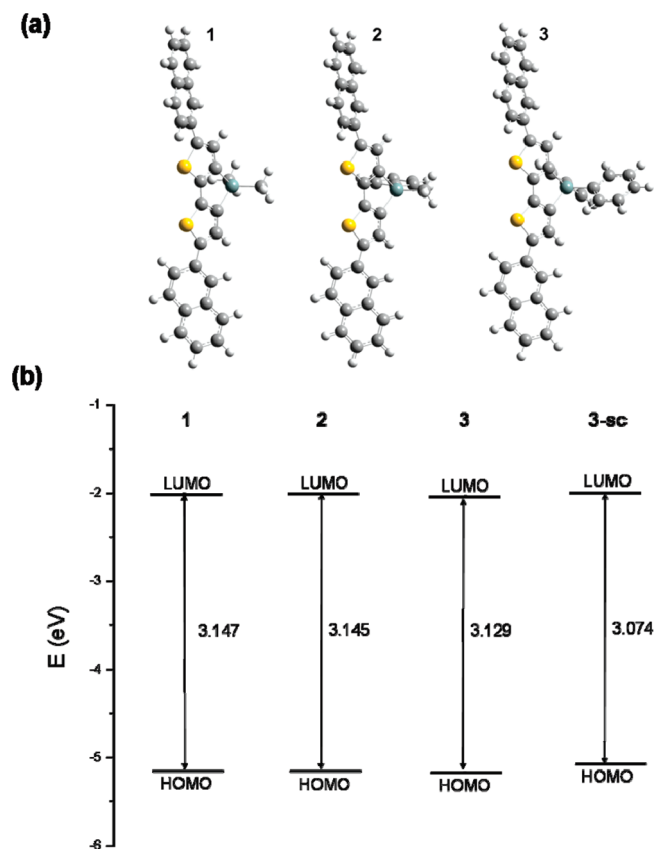


Figure 5. (a) Optimized geometries of 1–3 and (b) schematic representation of the frontier molecular orbitals for 1–3 and the single crystal structure of 3 (3-sc).

Table 2. Absorption, Emission, Thermal, and Electrochemical Data of Dithienosiloles

| | UV/vis (λ_{\max}/nm) | | emission (λ_{\max}/nm) | | $E_{\text{onset}}^{\text{ox}}$ (V) ^c | $\Phi_{\text{(PL)}}^d$ | T_g (°C) | T_m (°C) | T_d (°C) ^e |
|---|--|-------------------|--|------|--|------------------------|---------------|---------------|----------------------------|
| | solution ^a | film ^b | solution | film | | | | | |
| 1 | 421 | 425 | 481 | 521 | 0.60 | 0.32 | 225 | 325 | |
| 2 | 423 | 427 | 484 | 528 | 0.64 | 0.27 | 87 | 212 | 359 |
| 3 | 426 | 431 | 491 | 532 | 0.66 | 0.21 | | 301 | 383 |

^aIn CH_2Cl_2 . ^bPMMA-doped film. ^cVersus Fc/Fc^+ . ^dRelative to 9,10-diphenylanthracene ($\Phi_{\text{PL}} = 0.9$) in CH_2Cl_2 at room temperature (error range $\approx \pm 0.1$). ^e T_d , decomposition temperature, was defined as 5% of weigh loss under N_2 atmosphere.

measurements were conducted in CH_2Cl_2 , while the calculations were carried out *in vacuo*.

To further investigate the electronic effects caused by the addition of substituents at the silicon atom, cyclic voltammetry experiments were carried out using ferrocene (Fc/Fc^+) as the internal standard. Due to the limited range available in CH_2Cl_2 and the inability of our instrument to measure reliable reduction potentials in the region -2.0 to -3.5 V, we have obtained only reliable oxidation potentials for all compounds. Cyclic voltammetry measurements of 1, 2, and 3 in solution produced essentially identical results for oxidation, suggesting that the oxidation observed is mainly due to naphthyl and bithiophene of the DTS ring (see the Supporting Information). Oxidation wave potentials do not significantly change upon the nature of the substituents on the

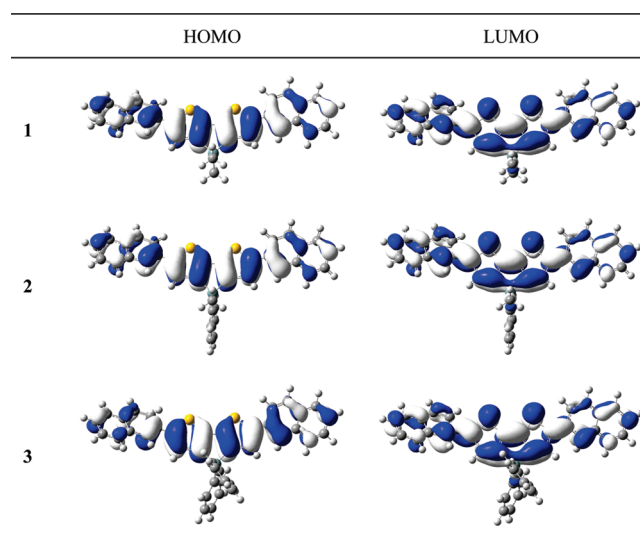


Figure 6. Isodensity surface plots of the HOMO and LUMO of 1–3 (isodensity value = 0.02 au).

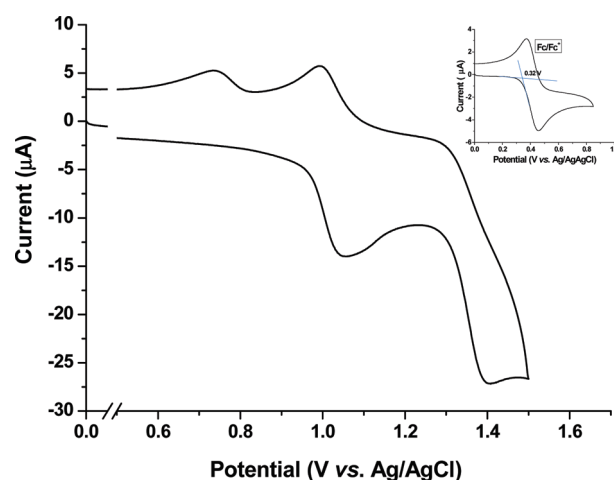


Figure 7. Cyclic voltammogram of 2 measured in $\text{CH}_3\text{CN}/\text{CH}_2\text{Cl}_2$ using Ag/AgCl (0.5 mM) as a reference electrode and Bu_4NPF_6 as an electrolyte at a scan rate of 100 mV/s. Inset: Fc/Fc^+ couple as internal standard.

Table 3. Calculated $S_0 \rightarrow S_1$ Excitation Energies (E), Oscillator Strengths (f), Configuration Compositions with CI Coefficient Larger than 0.2, and Experimental Absorption Band Maxima in Solution

| molecule | E (eV/nm) | f | composition (CI coefficient) | exptl λ_{\max} in sol. (nm) |
|----------|-------------|-------|---------------------------------|--|
| 1 | 3.31/375 | 1.091 | HOMO→LUMO (0.634) | 421 |
| 2 | 3.29/376 | 1.051 | HOMO→LUMO (0.633) | 423 |
| 3 | 3.28/378 | 1.003 | HOMO→LUMO (0.633) | 426 |

silicon atom. Upon anodic sweep in a mixture of CH_2Cl_2 and CH_3CN , a quasi-reversible and an irreversible oxidation are observed at 1.05 V (E_{pa1}), 1.40 V (E_{pa2}) for 1, 1.07 V (E_{pa1}), 1.39 V (E_{pa2}) for 2, and 1.08 V (E_{pa1}), 1.39 V (E_{pa2}) for 3, respectively (Figure 7). The onset potentials of oxidation for 1, 2, and 3 appeared at 0.92, 0.96, and 0.98 V, respectively (vs Ag/AgCl), corresponding to 0.60, 0.64, and 0.66 V (vs Fc/Fc^+). On the basis of these observations, the HOMO levels for 1, 2, and 3 were estimated using an oxidation potential of

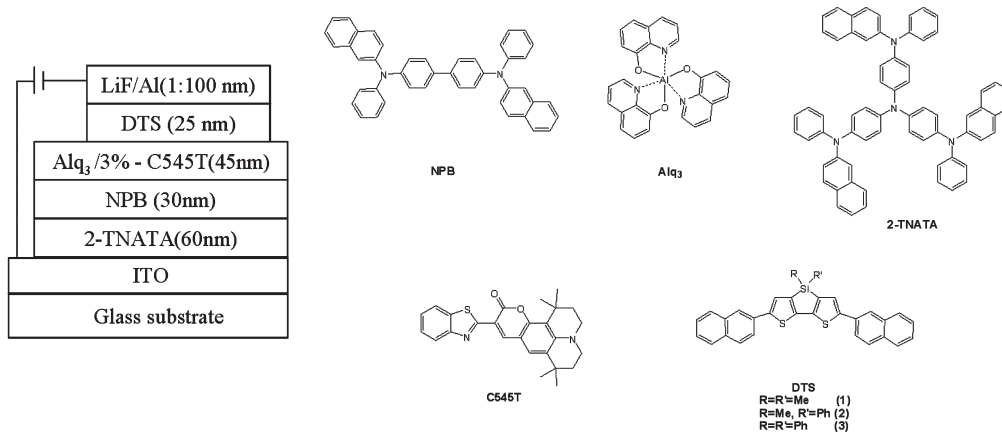


Figure 8. Device structure and molecular structures used in this study.

ferrocene/ferrocenium (4.8 eV below the vacuum level).²⁵ Therefore, the HOMO levels for **1**, **2**, and **3** are estimated to be -5.40 , -5.44 , and -5.46 eV, respectively. These values are lower than those of diaryl-spiro-dithienosiloles (4.9–5.0 eV) but higher than that of Alq₃ (5.7 eV), commonly used as an electron-transporting material in OLEDs. The LUMO levels were estimated from the tails of corresponding absorption spectra; the estimated values were -2.84 eV for **1**, -2.92 eV for **2**, and -2.96 eV for **3**, respectively. These results suggest that the electron-withdrawing effect from the phenyl group bound to the silicon atom has a significant influence on the LUMO energy rather than the HOMO energy. Furthermore, lowering the LUMO energy of **3** is in substantial agreement with red-shifted absorption.

OLDE Performance Based on Naphthylidithienosilole As the Electron-Transporting Material. To investigate the electroluminescence (EL) properties of **1**, **2**, and **3**, we fabricated a multilayer device with the configuration of ITO/2-TNATA (30 nm)/NPB(45 nm)/3%-C545T-doped Alq₃(45 nm)/DTS (25 nm)/LiF(100 nm)/Al(1 nm), where NPB is 4,4'-bis(*N*-phenyl-1-naphthylamino)biphenyl, 2-TNATA is 4,4',4''-tris(*N*-(2-naphthyl)-*N*-phenylamino)triphenylamine, C545T is 10-(2-benzothiazolyl)-1,1,7,7-tetramethyl-2,3,6,7-tetrahydro-1*H*,5*H*,11*H*-benzo[*l*]pyrano[6,7,8-*ij*]quinolizin-11-one, and Alq₃ is tris(8-hydroxyquinolato)aluminum(III). The layers of the device consist of ITO as the anode, 2-TNATA as the hole-injection layer, NPB as the hole-transporting layer, Alq₃:3%-C545T as the emitter, DTS as the electron-transporting layer, LiF as the electron-injection layer, and Al as the cathode, respectively (Figure 8). In this study, we chose Alq₃ as the host material, which is a prototypical host with a wide band gap for green OLEDs. In three EL devices, green emission originating from C545T was observed at 524 nm (λ_{\max}) (see Supporting Information). Based on the *I*–*V* characteristics (Figure 9), carrier-transporting properties were estimated and improved in the order **1** < **3** < **2**. In general, electron-transporting (ET) ability depends significantly on the LUMO energy level of the material used in ET layer. When an ET material has low-lying LUMO energy, electron injection from the cathode has been facilitated and ET ability has been improved as well. According to the electrochemical and absorption data, compound **3** has lower LUMO energy than in **1** and **2**. Thus, we envisioned that the carrier transporting of **3** would be improved more than that

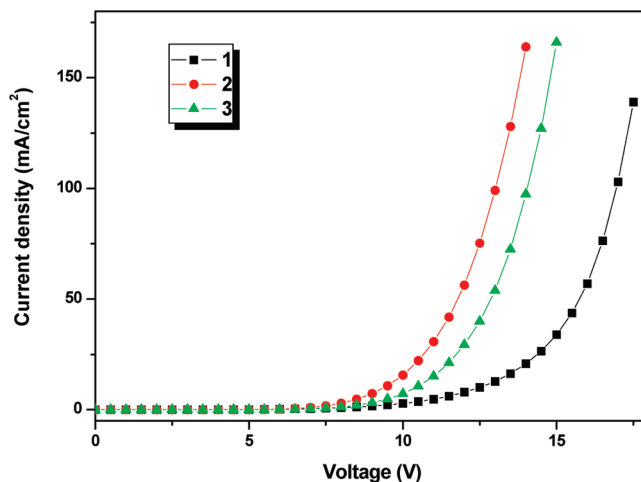


Figure 9. Voltage versus current-density characteristics based on **1** (squares), **2** (circles), and **3** (triangles).

Table 4. Electroluminescence Data^a

| compound | EL (λ_{\max} , nm) | turn-on voltage (V) ^b | luminescence (cd/m ²) at 40 mA/cm ² | efficiency (cd/A) ^c |
|-------------------------------|-----------------------------|----------------------------------|--|--------------------------------|
| 1 | 524 | 8.5 | 3535 | 7.98 |
| 2 | 524 | 7 | 3059 | 7.32 |
| 3 | 524 | 7.5 | 2804 | 7.03 |
| reference device ^d | 524 | 7 | 3133 | 7.74 |

^a Device structure: ITO/2-TNATA/NPB/Alq₃:C545T(3%)/DTS/LiF/Al. ^b Defined as 1 mA/cm². ^c At 3000 cd/m². ^d ITO/2-TNATA/NPB/Alq₃:C545T(3%)/Alq₃/LiF/Al.

of either **1** or **2** if compound **3** is used as the ET material in devices. However, a better carrier-transporting ability in **2** appeared. The reason for this phenomenon is not understood yet. Although the observed results deviate from our expectation, the carrier transporting tendency is matched with a previous report because the ET ability of **3** is much higher than that of **1**. Also, the difference of turn-on voltage between **2** and **3** turned out to be insignificant.

The operating voltage (defined as 1 mA/cm²) of the device is observed from 7 to 8.5 V. As shown in Figure 9 and Table 4, the device with **1** as ET materials showed better performance, exhibiting a luminescence efficiency of 7.98 cd/A (3000 cd/m²) with Commission Internationale de L'Éclairage (CIE) coordinates of $x = 0.31$ and $y = 0.65$ at a current density of 12.52 mA/cm².

(25) Lee, S. H.; Jang, B.-B.; Tsutsui, T. *Macromolecules* **2002**, *35*, 1356.

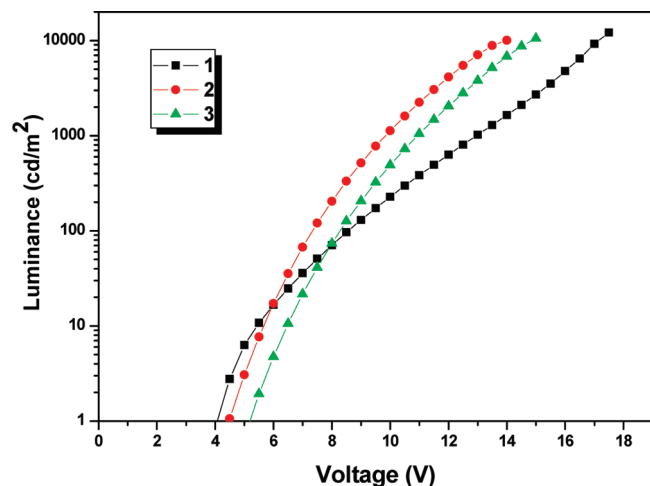


Figure 10. Voltage versus luminescence characteristics based on **1** (squares), **2** (circles), and **3** (triangles).

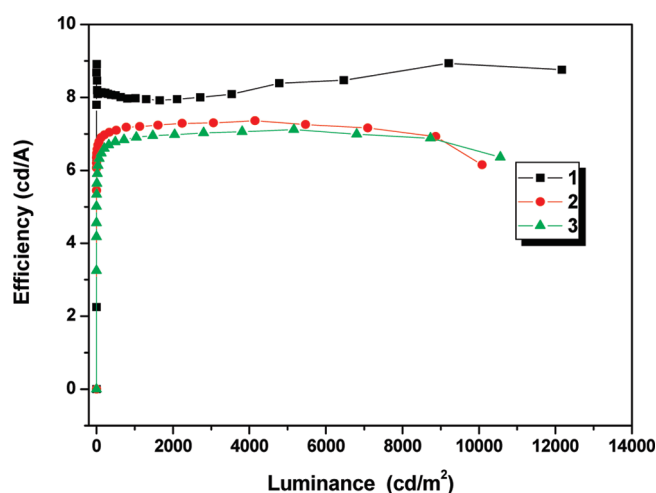


Figure 11. Luminescence versus current efficiency characteristics based on **1** (squares), **2** (circles), and **3** (triangles).

This result supports the fact that the device with DTS as electron transporter shows higher efficiency. Other EL characteristics using **2** and **3** are also presented in Figures 10 and 11, and their results are listed in Table 4. The device efficiency of **2** and **3** is lower than that of **1**: 7.32 cd/A (**2**), 7.03 cd/A (**3**) at 3000 cd/m². Further improvement and optimization of EL devices using **1**, **2**, and **3** are being investigated in our laboratory.

Conclusions. In summary, a series of DTS-based green luminescent compounds have been synthesized and characterized, including their thermal, photophysical, and electrochemical properties and the nature of their solid-state structures. The DTS linkage incorporated with naphthyl segments can give rise to several distinct characteristics, impacting their solid-state structures, electrochemical behavior, and photoluminescence. As expected, the substituent on the Si atom slightly perturbed the absorption, redox potentials, and photo- and electroluminescent efficiency. In particular, a low-lying LUMO in **3** was observed compared with those of **1** and **2**, indicating that the phenyl substituents on the Si atom induced a relative diminution of the band gap. Compound **1** used as an ET material exhibits a bright emission in a multilayered EL device.

Experimental Section

General Considerations. All reagents were purchased from commercial sources without further purification unless otherwise noted. All solvent were freshly distilled from appropriate drying agents prior to use. Conventional Schlenk techniques were used, and reactions were carried out under a nitrogen atmosphere unless otherwise noted. Starting materials, 3,3',5,5'-tetrabromobithiophene (**A**), 3,3'-dibromo-5,5'-bis(trimethyl silyl)-2,2'-bithiophene (**B**), and 4,4-dimethyl-, 4,4-methylphenyl-, and 4,4-diphenyl-2,6-bis(trimethylsilyl)dithienosilole (**C**) were prepared as reported earlier.²⁶

Measurements. ¹H NMR spectra were recorded with a Bruker Avance 300 or 400 MHz spectrometer. The absorption and photoluminescence spectra were recorded on a Perkin–Elmer Lambda 2S UV–visible spectrometer and a Perkin LS fluorescence spectrometer, respectively. Cyclic voltammetry was carried out with a BAS 100B (Bioanalytical Systems, Inc.) under a nitrogen atmosphere in a one-compartment electrolysis cell consisting of a platinum wire working electrode, a platinum wire counter electrode, and a quasi Ag/AgCl reference electrode. Cyclic voltammograms were monitored at scan rates of either 100 or 50 mV s^{−1} and recorded in distilled dichloromethane. The concentration of the complex was maintained at 0.5 mM or less, and each solution contained 0.1 M of tetrabutyl ammoniumhexafluorophosphate (TBAP) as an electrolyte. The ferrocenium/ferrocene couple ($E_{\text{onset}}^{\text{ox}}$: 0.32 V) was used as the internal standard.

Theoretical Calculations. The geometry optimizations in the ground state were performed at the density functional theory (DFT) level with the B3LYP exchange–correlation functional and a 6-311** basis set. The molecular orbital energy levels were obtained at the same level of calculations. The vertical excitation energies from S₀ to S₁ were evaluated using time-dependent DFT (TDDFT) with the B3LYP/6-311G**. For comparison, the molecular orbital energy levels of the single-crystal structure of **3** (**3-sc**) were also computed. All the calculations were carried out using the Gaussian 03 package,²⁷ and visualizations were made with GaussView 5.²⁸

X-ray Crystallographic Analysis. All data were collected on a Bruker SMART APEX II ULTRA diffractometer equipped with graphite-monochromated Mo K α radiation ($\lambda = 0.71073$ Å) generated by a rotating anode. The cell parameters for the compounds were obtained from a least-squares refinement of the spot (from 36 collected frames). Data collection, data reduction, and semiempirical absorption corrections were carried out using the software package APEX2.²⁹ All of the calculations for the structure determination were carried out using the SHELXTL package.³⁰ All non-hydrogen atoms were refined anisotropically, and all hydrogen atoms were placed in

(26) (a) Yui, K.; Aso, Y.; Otsubo, T.; Ogura, F. *Bull. Chem. Soc. Jpn.* **1989**, *62*, 1539. (b) Ohshita, J.; Nodono, M.; Kai, H.; Watanabe, T.; Kunai, A.; Komaguchi, K.; Shiotani, M.; Adachi, A.; Okita, K.; Harima, Y.; Yamashita, K.; Ishikawa, M. *Organometallics* **1999**, *18*, 1453.

(27) Frisch, M. J.; Trucks, G. W.; Schlegel, H. B.; Scuseria, G. E.; Robb, M. A.; Cheeseman, J. R.; Montgomery, J. A., Jr.; Vreven, T.; Kudin, K. N.; Burant, J. C.; Millam, J. M.; Iyengar, S. S.; Tomasi, J.; Barone, V.; Mennucci, B.; Cossi, M.; Scalmani, G.; Rega, N.; Petersson, G. A.; Nakatsuji, H.; Hada, M.; Ehara, M.; Toyota, K.; Fukuda, R.; Hasegawa, J.; Ishida, M.; Nakajima, T.; Honda, Y.; Kitao, O.; Nakai, H.; Klene, M.; Li, X.; Knox, J. E.; Hratchian, H. P.; Cross, J. B.; Adamo, C.; Jaramillo, J.; Gomperts, R.; Stratmann, R. E.; Yazyev, O.; Austin, A. J.; Cammi, R.; Pomelli, C.; Ochterski, J. W.; Ayala, P. Y.; Morokuma, K.; Voth, G. A.; Salvador, P.; Dannenberg, J. J.; Zakrzewski, V. G.; Dapprich, S.; Daniels, A. D.; Strain, M. C.; Farkas, O.; Malick, D. K.; Rabuck, A. D.; Raghavachari, K.; Foresman, J. B.; Ortiz, J. V.; Cui, Q.; Baboul, A. G.; Clifford, S.; Cioslowski, J.; Stefanov, B. B.; Liu, G.; Liashenko, A.; Piskorz, P.; Komaromi, I.; Martin, R. L.; Fox, D. J.; Keith, T.; Al-Laham, M. A.; Peng, C. Y.; Nanayakkara, A.; Challacombe, M.; Gill, P. M. W.; Johnson, B.; Chen, W.; Wong, M. W.; Gonzalez, C.; Pople, J. A. *Gaussian 03*; Gaussian, Inc.: Pittsburgh, PA, 2003.

(28) *GaussView 5*; Gaussian, Inc.: Pittsburgh, PA, 2009.

(29) Bruker. *APEX2* Version 2009.1-0 Data Collection and Processing Software; Bruker AXS Inc.: Madison, WI, 2008.

(30) Bruker. *SHELXTL-PC* Version 6.22 Program for Solution and Refinement of Crystal Structures; Bruker AXS Inc.: Madison, WI, 2001.

idealized positions and refined isotropically in a riding manner along with the their respective parent atoms. Relevant crystal data collection and refinement data for the crystal structure of **3** are summarized in Table 1.

Fabrications of Electroluminescent Devices. Electroluminescent devices were fabricated by vapor depositing organic layers onto a glass substrate precoated with indium–tin oxide (ITO) with a sheet resistance of 10 Ω /cm. The substrate was washed, dried, and then immediately loaded into the evaporation system. The organic and metal cathode layers were grown in the chamber at 1×10^{-7} and 6×10^{-7} Torr without breaking the vacuum, respectively. The deposition process started with a 30 nm thick hole-injection layer of 2-TNATA, a 45 nm thick hole-transporting layer of NPB, followed by a 45 nm thick layer of C545T-3%:Alq₃ (dopant:host), a 25 nm thick electron-transporting layer of tris(8-hydroxyquinolinato)aluminum(III) (Alq₃), and finally a metallic LiF/Al layer. The emission area of the devices was 9 mm². After deposition, the device was measured immediately without encapsulation. The EL spectra and current–voltage–luminescence characteristics were measured with a Minolta CS 1000 photometer and a computer-controlled dc power supply under ambient conditions. The emission area of the devices is 0.09 cm², as determined by the overlap area of the anode and the cathode.

Synthesis of 5,5'-Diiododithienosilole (D). To a 40 mL ether solution of 2,6-bis(trimethylsilyl)dithienosilole (5.45 mmol) was added dropwise 11.99 mL (11.99 mmol; 1.0 M in CH₂Cl₂) of iodine monochloride at –90 °C, and the resulting mixture was stirred for 2 h at this temperature in the dark. After the solvent was removed under reduced pressure, the residue was washed with either methanol or ethanol to give yellow solids, which were recrystallized from chloroform. Data for 5,5'-diiodo-1,1-dimethyldithienosilole: 65% yield. ¹H NMR (CDCl₃): δ 7.20 (s, 2H), 0.39 (s, 6H). Anal. Calcd for C₁₀H₈I₂S₂Si: C, 25.33; H, 1.70. Found: C, 25.31; H, 1.73. Data for 5,5'-diiodo-1-methyl-1-phenyldithienosilole: 67% yield. ¹H NMR(CDCl₃): δ 7.45–7.42 (m, 2H), 7.34–7.27 (m, 3H), 7.19 (s, 2H), 0.61 (s, 3H). Anal. Calcd for C₁₅H₁₀I₂S₂Si: C, 33.60; H, 1.88. Found: C, 33.57; H, 1.84. Data for 5,5'-diiodo-1,1'-diphenyldithienosilole: 70% yield. ¹H NMR(CDCl₃): δ 7.60–7.57 (m, 2H), 7.45–7.37 (m, 3H), 7.34 (s, 1H). Anal. Calcd for C₂₀H₁₂I₂S₂Si: C, 40.15; H, 2.02. Found: C, 40.17; H, 2.03.

General Preparation of 1–3. 2-Naphthyllithium was prepared from 2-bromonaphthalene (0.21 g, 1.05 mmol) by treatment with *n*-BuLi (1.05 mmol, 1.6 M in hexane) at –78 °C for 15 min followed by warming to room temperature. This compound was used immediately for the preparation of tri(2-naphthyl)indium. To a solution of InCl₃ (0.076 g, 0.35 mmol) in THF (5 mL)

at –78 °C was added 2-naphthyllithium (1.05 mmol in Et₂O) under a nitrogen atmosphere, and the mixture was stirred for 30 min. After the cooling bath was removed, the reaction mixture was warmed to room temperature for 30 min. The solution of tri(2-naphthyl)indium was subsequently added to a mixture of Pd(dppf)Cl₂ (0.031 g, 4% mol) and the corresponding 5,5'-diiododithienosiloles (0.5 mmol) in THF under a nitrogen atmosphere. The reaction mixture was stirred at 80 °C for 10 h until the starting material was consumed on TLC. After being cooled to room temperature, the reaction mixture was quenched by water. The aqueous layer was extracted with CH₂Cl₂, and the combined organic layers were sequentially washed with saturated aqueous NaCl (20 mL), dried with MgSO₄, filtered, and concentrated under reduced pressure. The residue was purified by silica gel column chromatography using CH₂Cl₂ and hexane to give the title compounds (70–80% GC yield, 50–60% isolated yield) as an orange-red solid.

Data for 5,5'-bis(2-naphthyl)-1,1-dimethyldithienosilole (1): 49% yield. ¹H NMR (CDCl₃): δ 7.98 (s, 2H), 7.79–7.71 (m, 8H), 7.43–7.40 (m, 6H), 0.45 (s, 6H). ¹³C NMR (CDCl₃): δ 149.4, 146.4, 144.9, 134.5, 133.4, 132.8, 130.2, 129.4, 128.8, 128.5, 127.4, 126.7, 125.0, 124.6, –2.5. MALDI-TOF MS (*m/z*): 474.0. Anal. Calcd for C₃₀H₂₂S₂Si: C, 75.90; H, 4.67. Found: C, 75.88; H, 4.59.

Data for 5,5'-bis(2-naphthyl)-1-methyl-1-phenyldithienosilole (2): 57% yield. ¹H NMR (CDCl₃): δ 8.05 (s, 2H), 7.85–7.80 (m, 6H), 7.77–7.76 (m, 2H), 7.68–7.66 (m, 2H), 7.50–7.44 (m, 6H), 7.40–7.38 (m, 3H), 0.81 (s, 3H). ¹³C NMR (CDCl₃): δ 149.7, 146.4, 143.1, 134.9, 134.1, 133.7, 133.1, 132.3, 128.9, 128.7, 128.4, 128.1, 127.0, 126.4, 126.3, 124.6, 124.2, –4.7. MALDI-TOF MS (*m/z*): 536.1. Anal. Calcd for C₃₀H₂₂S₂Si: C, 78.31; H, 4.51. Found: C, 78.40; H, 4.55.

Data for 5,5'-bis(2-naphthyl)-1,1-diphenyldithienosilole (3): 50% yield. ¹H NMR (CDCl₃): δ 8.07 (s, 2H), 7.86–7.78 (m, 8H), 7.76–7.74 (m, 4H), 7.50–7.39 (m, 12H). ¹³C NMR (CDCl₃): δ 150.2, 146.7, 141.6, 135.9, 134.1, 133.0, 132.3, 131.9, 130.9, 129.0, 128.7, 128.4, 126.5, 126.3, 124.6, 124.3. MALDI-TOF MS (*m/z*): 598.1. Anal. Calcd for C₄₀H₂₆S₂Si: C, 80.23; H, 4.38. Found: C, 80.16; H, 4.41.

Acknowledgment. This research was supported by the Basic Science Research Program through the National Research Foundation of Korea (NRF) funded by the Ministry of Education, Science and Technology (2009-0072468).

Supporting Information Available: This material is available free of charge via the Internet at <http://pubs.acs.org>.